

UWB Mixed-Signal Transform-Domain Direct-Sequence Receiver

Sebastian Hoyos and Brian M. Sadler, *Fellow, IEEE*

Abstract— We consider a mixed-signal ultra wideband (UWB) direct-sequence spread-spectrum (DS-SS) receiver. The receiver expands the signal over a basis set, and then operates on the basis coefficients. An analog computation of the basis coefficients efficiently parallelizes the signal for digital processing, relaxing the sampling requirements and enabling parallel digital processing at a much lower rate. Bit error rate (BER) performance is evaluated, as well as distortion due to basis truncation. The parallel processing also facilitates efficient interference mitigation. Various models for interference including adjacent multicarrier interference are developed and analyzed. Several simulation results confirm the analysis and provide insight into quantization error, basis truncation distortion, and the impact of the UWB channel. We show that in the AWGN uncoded case for SNR < 10 dB, the receiver can be operated at almost half the Nyquist rate with only 1 dB of performance loss. Moreover, when a common convolutional code is employed, the aggregate sampling rate can be 37.5 % lower than Nyquist rate with little loss in receiver performance.

Index Terms— Analog to digital conversion, broadband wireless communications, direct sequence spread spectrum, ultra-wideband communications.

I. INTRODUCTION

ULTRA-WIDEBAND (UWB) systems face significant implementation challenges, including achieving sufficient front-end dynamic range to support desired receiver processing gain and rejection of large narrowband interferers (NBI), and overcoming channel-induced distortion. These goals need to be accomplished with manageable power consumption and complexity, while pushing achievable bandwidths. Digital solutions are flexible and desirable, yet receiver algorithms may be very complex, and high speed analog-to-digital converters (ADC) have limited dynamic range. These issues motivate unconventional receiver designs, such as parallel schemes that utilize analog channelization or time interleaving followed by sampling [1]–[5]. These approaches allow the use of lower

resolution in each channel with a reasonable compromise in performance degradation. In addition, when a single bit is used for the quantization, the ADC complexity is greatly reduced [6], [7].

In this paper we consider an approach that utilizes analog basis expansion of the input signal, followed by parallel sampling of the basis coefficients [8]. The number of basis coefficients, and the rate at which they are estimated, provides a flexible tradeoff. Many basis choices are possible, and the use of a Fourier basis yields a solution that scales with bandwidth. Based on this, we develop a direct-sequence (DS) UWB receiver that accepts the basis coefficients as input. This method does not require signal reconstruction, enables parallel digital signal processing, and leads to considerable complexity reduction. Moreover, we show that the receiver can operate at a sub-Nyquist sampling rate for practical SNRs (SNRs < 10 dB or so), and still achieve a performance very close to Nyquist rate digital receivers.

The proposed mixed-signal parallel architecture facilitates new directions and ways of implementing desired signal processing in the DS receiver, such as multi-user detectors. For example, we illustrate the ideas by considering power-mismatched adjacent channel interference removal. This problem will become increasingly apparent with short range UWB personal area networks.

The paper is organized as follows. The DS signal and channel models are set up in Section II. We describe the signal expansion and sampling ideas in Section III. In Section IV we develop the linear model for the received signal and several candidates for the detection based on the basis coefficients. Interference mitigation schemes that benefit the proposed signal expansions are introduced in V. In Section VI we derive coded BER expressions, including the dependence on the number of basis coefficients and basis truncation error effects. Section VII provides simulation results, where we examine receiver performance as a function of various system parameters. In particular, we show that a coded system can be under-sampled, yet achieve optimal BER performance. Section VIII provides conclusions.

II. TRANSMITTED SIGNAL AND CHANNEL MODEL

Assume that a channel encoder¹ with rate $R_c = I/J$ provides the sequence of coded bits $c_j \in [0, 1]$. The pseudorandom (PN) sequence $b_j \in [0, 1]$ is impressed on the transmitted signal by multiplying each coded bit by the j th bit of the PN

¹The signal model presented here is valid for block codes as well as for convolution codes.

Manuscript received December 26, 2005; revised October 30, 2006; accepted February 6, 2007. The associate editor coordinating the review of this paper and approving it for publication was Z. Tian. This manuscript was prepared through collaborative participation in the Communications and Networks Consortium sponsored by the U. S. Army Research Laboratory under the Collaborative Technology Alliance Program, Cooperative Agreement DAAD19-01-2-0011. The U. S. Government is authorized to reproduce and distribute reprints for Government purposes notwithstanding any copyright notation thereon. The views and conclusions contained in this document are those of the authors and should not be interpreted as representing the official policies, either expressed or implied, of the Army Research Laboratory or the U. S. Government.

S. Hoyos is with the Department of Electrical and Computer Engineering, Texas A&M University, 318G WERC 3128 TAMU, College Station, TX 77843-3128 USA (e-mail: hoyos@ece.tamu.edu).

B. M. Sadler is with the Army Research Laboratory, 2800 Powder Mill Rd., Adelphi, MD 20783 USA (e-mail: bsadler@arl.army.mil).

Digital Object Identifier 10.1109/TWC.2007.051069.

sequence [9]. The transmitted signal can be expressed as

$$s(t) = \sum_{j=-\infty}^{\infty} (2c_j - 1)(2b_j - 1) \sqrt{E_s} p_{tx}(t - jT_p), \quad (1)$$

where $p_{tx}(t)$ is a unit energy transmitted pulse with duration T_p and E_s is the transmit energy per coded bit c_j . A ternary spreading model can also be employed for episodic transmission [10].

The transmitted signal is corrupted by frequency selective multipath and additive noise after propagation through the channel $h(t)$. The received signal can be represented as the convolution of the transmitted signal and the linear channel model

$$\begin{aligned} r(t) &= s(t) * h(t) \\ &= \sum_{j=-\infty}^{\infty} (2c_j - 1)(2b_j - 1) \sqrt{E_s} p_{rx}(t - jT_p) + z(t) \\ &= \sum_{j=-\infty}^{\infty} a_j \sqrt{E_s} p_{rx}(t - jT_p) + z(t), \end{aligned} \quad (2)$$

where $a_j = (2c_j - 1)(2b_j - 1) \in [-1, 1]$, and $*$ denotes convolution. The received pulses are denoted as $p_{rx}(t)$, which may differ from the transmitted pulse $p_{tx}(t)$ due to waveform distortion introduced by the frequency selectivity of the medium, as well as possibly being altered by the receive antenna transfer function that is often modeled as differentiation [11]. The additive noise $z(t)$ is modeled as a white, zero mean, Gaussian random process, with two-sided spectral density $N_o/2$.

III. BASIS EXPANSION AND SAMPLING

The received signal $r(t)$ is decomposed every T_c seconds into N components that are obtained via projection over the basis $\Phi_n(t) \big|_{n=0}^{N-1}$. The coefficients $R_{m,n} \big|_{m=0}^{M-1} \big|_{n=0}^{N-1}$ are given by

$$R_{m,n} = \langle r(t), \Phi_n(t) \rangle_{m, T_c, T_s} = \int_0^{T_c} r(t + mT_s) \Phi_n^*(t) dt. \quad (3)$$

At the end of each integration time T_c^2 , the coefficients reach a value that is fed to a set of quantizers $Q_n \big|_{n=0}^{N-1}$, one for each coefficient, which return the digital words $\hat{R}_{m,n} \big|_{m=0}^{M-1} \big|_{n=0}^{N-1}$. Let the n th quantizer Q_n have 2^{b_n} output levels, where $b_n \big|_{n=0}^{N-1}$ is the number of bits used to obtain the quantized set of coefficients. The windows of duration T_c can overlap to avoid the high frequency artifacts caused by windowing, so the time shift T_s in (3) is less than or equal to the integration time T_c . This means that if a period T of the signal $r(t)$ has to be windowed in M segments of duration T_c , with overlapping time $T_c - T_s$ or equivalently overlapping percentage $\text{OVR} = \frac{T_c - T_s}{T_c}$, the equation $T_c + (M - 1)T_s = T$

²In our notation, T_c is the integration time for the basis coefficient calculation in (3), and T_p is the pulse or chip time.

holds and the following relations can be derived

$$\text{OVR} = \frac{T_c - T_s}{T_c} = \frac{T - MT_s}{T_c} \quad (4)$$

$$M = \frac{T - \text{OVR} \cdot T_c}{T_s} \quad (5)$$

$$M = \frac{T - \text{OVR} \cdot T_c}{(1 - \text{OVR})T_c}. \quad (6)$$

IV. PROPOSED TRANSFORM-DOMAIN DIRECT-SEQUENCE RECEIVER

In order to obtain an estimate of the transmitted bit a_i (the sign of the i th chip) from the set of coefficients provided by the quantized basis coefficients, we begin by expressing the receiver structure as a linear filtering problem in the same transform-domain in which $r(t)$ has been expanded. To obtain a vector notation we group the samples in (3) into the $L \times 1$ vector $\mathbf{r} = [r_0 \cdots r_{L-1}]^T$ where $L = MN$ and the l th component, $l = mN + n$, is given by $r_l = R_{m,n}$. We assume that a period of T seconds of the signal $r(t)$, containing K chips $\mathbf{a} = [a_0 \cdots a_{K-1}]^T$ of duration T_p each, are represented in the vector \mathbf{r} . An estimate of \mathbf{a} , namely $\hat{\mathbf{a}}$, is obtained via the linear receiver $K \times L$ matrix \mathbf{H} as

$$\hat{\mathbf{a}} = \mathbf{H}\mathbf{r}. \quad (7)$$

The choice of \mathbf{H} plays a fundamental roll in the performance and complexity of the digital baseband of this receiver. Next, we explicitly write the samples $R_{m,n}$ as,

$$R_{m,n} = \sum_{k=1}^K \langle f_k(t), \Phi_n(t) \rangle_{m, T_c, T_s} + \langle z(t), \Phi_n(t) \rangle_{m, T_c, T_s}, \quad (8)$$

where $f_k(t) = a_k p_{rx}(t - kT_p)$ is the k th received pulse that conveys the chip a_k . Thus,

$$\begin{aligned} R_{m,n} &= \sum_{k=1}^K a_k \langle p_{rx}(t - kT_p), \Phi_n(t) \rangle_{m, T_c, T_s} \\ &\quad + \langle z(t), \Phi_n(t) \rangle_{m, T_c, T_s}. \end{aligned} \quad (9)$$

To obtain a vector notation we define the $L \times K$ matrix \mathbf{G} whose components are given by $g_{l,k} = \langle p_{rx}(t - kT_p), \Phi_n(t) \rangle_{m, T_c, T_s}$, where $l = mN + n$. We also define the $L \times 1$ noise vector \mathbf{z} whose components are $z_l = \langle z(t), \Phi_n(t) \rangle_{m, T_c, T_s}$. Thus we can write,

$$\mathbf{r} = \mathbf{G}\mathbf{a} + \mathbf{z}. \quad (10)$$

The problem now is to find the matrix \mathbf{H} in (7) that provides an estimate to the problem described in (10). This is a straightforward linear problem where we can easily identify 3 solutions: the Minimum Mean-Squared-Error (MMSE), the Least Squares (LS), and the Matched-Filter (MF) solutions, given by the following expressions:

$$\mathbf{H}_{\text{MMSE}} = \Sigma_a \mathbf{G}^H (\mathbf{G} \Sigma_a \mathbf{G}^H + \mathbf{Z})^{-1} \quad (11)$$

$$\mathbf{H}_{\text{LS}} = \begin{cases} (\mathbf{G}^H \mathbf{G})^{-1} \mathbf{G}^H & \text{if } L > K; \\ \mathbf{G}^{-1} & \text{if } L = K; \\ \mathbf{G}^H (\mathbf{G} \mathbf{G}^H)^{-1} & \text{if } L < K. \end{cases} \quad (12)$$

$$\mathbf{H}_{\text{MF}} = \mathbf{G}^H, \quad (13)$$

where $\Sigma_a = E[\mathbf{a}\mathbf{a}^H]$ and $\mathbf{Z}_z = E[\mathbf{z}\mathbf{z}^H]$. \mathbf{H}_{MMSE} is optimal in the MSE sense, while \mathbf{H}_{LS} is maximum likelihood when the components of the noise vector \mathbf{z} are independent. On the other hand \mathbf{H}_{MF} is suboptimal but straightforward and has very low complexity. The performance of the LS solution for $L = K$ and $L > K$ is also optimal MMSE in the uncolored noise case and suboptimal in the colored case. For $L < K$ the LS exhibits poor performance while still having high complexity (not shown here), whereas the MF solution has very low complexity and so of great interest if its performance is acceptable. For this reason, in Section VI we focus on the derivation of the matched filter performance for the coded-system case.

Note that the linear formulation in (10) includes inter-symbol interference (ISI) between the received pulses $f_k(t) = a_k p_{rx}(t - kT_p)$, so the matrix \mathbf{H} in (7) will perform both signal detection and equalization. The trade-off here is the amount of data processed by \mathbf{H} when simultaneously estimating K chips in the $T = KT_p$ signal detection time. Since the receiver has N parallel paths, the sampling rate for each path will be N times lower than if a Nyquist rate time-domain ADC were used to sample the signal. We will show that the sampling rate may be further lowered (below Nyquist) without significant BER penalty if the truncation error is negligible compared with the additive noise, or if the incurred SNR degradation can be mitigated by the channel decoder. Next, we show that the receiver parallelization can be exploited to add robustness to adjacent channel interference.

V. INTERFERENCE MITIGATION

The fundamental difference between the receiver front-end introduced here, and the conventional single ADC architectures, is the way sampling of the received signal is performed. Folding of the signal spectrum introduced by time-domain sampling produces the classical frequency aliasing effect. If the front-end frequency selectivity of a conventional receiver does not provide the required attenuation of the adjacent frequencies, the remaining unknown and undesired adjacent channel interference will fold into the signal band and may seriously distort the discrete-time representation of the signal. We observe that by using the orthogonality principle in the frequency domain, we can select signals with great accuracy even if strong interferers are nearby. Unfortunately, there are practical limitations to this solution. The number of frequency samples that can be taken is limited to just a few (e.g., 10 frequency samples is a relatively large number with current technology) because of the complexity in the parallel bank of mixers and integrators needed. This limitation requires us to perform frequency sampling over short time windows, that in turn produces bandwidth expansion due to convolution in the frequency domain. This frequency expansion implies overlapping (aliasing) in the frequency domain, i.e., loss of orthogonality. The loss of orthogonality causes the adjacent, as well as in-band, interferers to overlap with the signal of interest producing destructive aliasing. We note that the amount of frequency overlapping due to windowing is a known quantity that is inversely proportional to the time duration of the window, and this is fundamentally different from the folding phenomenon of time-domain sampling. In

order to have the complete picture, we require the input signal frequency range, as well as the range that produces the aliasing due to frequency expansion. The digital baseband processes the frequency samples and can provide estimates of both the signal of interest and the interferers that were observed in the adjacent channels. This line of reasoning holds for any basis selection, noting that generally the harmonics involved in the aliasing must be taken into account as well.

To elaborate, we denote $i(t)$ the additive interference present in the received signal $r(t)$. Now, $R_{m,n}$ can be expressed as,

$$R_{m,n} = \sum_{k=1}^K a_k \langle p_{rx}(t - kT_p), \Phi_n(t) \rangle_{m, T_c, T_s} + \langle i(t), \Phi_n(t) \rangle_{m, T_c, T_s} + \langle z(t), \Phi_n(t) \rangle_{m, T_c, T_s}, \quad (14)$$

which means that the sample $R_{m,n}$ will be affected by the amount of correlation between $i(t)$ and $\Phi_n(t)$ collected by the term $\langle i(t), \Phi_n(t) \rangle_{m, T_c, T_s}$. If $i(t)$ were known, then theoretically it could be removed from $R_{m,n}$ and have no impact. However, in practice, $i(t)$ is either completely unknown or partially known. We show next that partial knowledge of $i(t)$ can be just enough to completely remove the negative effect of $i(t)$. In particular, we consider the case in which $i(t)$ is adjacent channel interference.

A. Adjacent Channel Interference

Multichannel designs are emerging to efficiently allocate multiple users in increasingly large bandwidths, as is the case with UWB [12]. Attenuation of the adjacent channel at the front-end of the receiver is crucial to avoid catastrophic aliasing after time-domain sampling. As the number of users grows, the adjacent channel problem becomes more important, especially when there is large variability in interference power levels due to mobility. In some cases, the neighboring nodes may be very close, such as with UWB personal area networks. To find a mathematical representation that includes adjacent channel-interference effects, we assume that at each side of a central channel of interest, C adjacent channels are separated by the frequency ΔF . We assume also that the signal has been demodulated to baseband, so a low-pass representation of the signals are presented to the receiver. In view of (14), the samples $R_{n,m}$ of the new multichannel signal can be expressed as

$$R_{m,n} = \sum_{k=1}^K a_k \langle p_{rx}(t - kT_p), \Phi_n(t) \rangle_{m, T_c, T_s} + \sum_{c=1}^C \sum_{k=1}^{K^{(L)}} a_k^{(L,c)} \left\langle \begin{matrix} p_{rx}^{(L,c)}(t - kT_p) \\ e^{-j2\pi c \Delta F} \Phi_n(t) \end{matrix} \right\rangle_{m, T_c, T_s} + \sum_{c=1}^C \sum_{k=1}^{K^{(R)}} a_k^{(R,c)} \left\langle \begin{matrix} p_{rx}^{(R,c)}(t - kT_p) \\ e^{j2\pi c \Delta F} \Phi_n(t) \end{matrix} \right\rangle_{m, T_c, T_s} + \langle z(t), \Phi_n(t) \rangle_{m, T_c, T_s}, \quad (15)$$

where the symbols and pulses of the C right and C left channels are distinguished by the super-indices (R) and (L) , respectively. Note that if the basis functions are made orthogonal to the adjacent interferer channels, the samples $R_{n,m}$

would not experience any interference. In practice, perfect orthogonality over all the adjacent frequencies cannot be achieved with finite time processing. Thus, some interference will be captured during the signal expansion and sampling. However, using (15) the mechanism by which this adjacent interference affects our signal expansion coefficients can be accurately modelled. In fact, the only unknowns in (15) are the adjacent channel symbols $a^{(R,c)}$ and $a^{(L,c)}$, and the number of interferers per channel $K^{(L)}$ and $K^{(R)}$. Although the pulses p_{rx} , $p_{rx}^{(L,c)}$ and $p_{rx}^{(R,c)}$ are initially unknown, they can be learned via training. With these estimates in hand, the problem is reduced to estimating the symbols of interest a_k and a portion of the adjacent symbols $a_k^{(R,c)}$ and $a_k^{(L,c)}$. The exact number of estimation symbols K' will be bounded by $K' \leq K + 2C(K^{(L)} + K^{(R)})$. This leads to a performance-complexity trade-off in the linear estimates in Eqns. (7) and (11-13). To enhance the detector performance, we need to increase $L = MN = K$ to $L' = M'N' = K'$. If N is increased, i.e., the parallel paths are increased, the trade-off is a linear increase in the amount of hardware. On the other hand, if M is increased, T_c decreases proportionally which implies an increase in the speed of the parallel ADCs.

1) *Mitigation of Adjacent Multicarrier Interference:* Besides DS signals, multicarrier signals may populate the spectrum. While DS signals are distinguished by choice of orthogonal spreading codes, multicarrier signals may be orthogonal due to their frequency separation. However, poorly attenuated adjacent multicarrier channels can fold into the DS signal of interest. The interference produced by adjacent multicarrier channels may be one of the most limiting performance factors for DS receivers. In band interference is of course also problematic, and we show that it can be also taken into account in the next formulation. To elaborate, the carriers are given by,

$$p_{rx}^{(L,c)} = e^{-j2\pi c \Delta F_c t} \quad (16)$$

$$p_{rx}^{(R,c)} = e^{j2\pi c \Delta F_c t}, \quad (17)$$

where the intercarrier spacing is denoted ΔF_c . The carrier frequency spacing may be known a priori (e.g., $\Delta F_c = 4.125$ MHz in UWB, and $\Delta F_c = 0.3125$ MHz in WiFi). In Section VII we present a set of simulations that demonstrate the performance of this interference mitigation scheme.

VI. BIT ERROR RATE ANALYSIS OF THE TRANSFORM-DOMAIN MATCHED FILTER SOLUTION IN A CODED-SYSTEM

Fig. 1 illustrates the mixed-signal receiver architecture. The unquantized output of the demodulator is denoted as \hat{a}_j , $1 \leq j \leq J$, and the estimates are obtained after multiplication with the PN sequence c_j , $1 \leq j \leq J$. Without loss of generality, we assume that the all-zero code word of a linear binary (J, I) block code is transmitted³ [9]. A soft decision decoder computes the correlation metrics (CM) ,

$$CM_i = \sum_{j=1}^J c_{ij} \hat{a}_j, \quad i = 1, 2, \dots, 2^I, \quad (18)$$

³We will show later that this analysis is also valid for convolutional codes.

where c_{ij} denotes the j th bit in the i th code word. In the following we extend the simple matched filter receiver described in (13). In order to express the matched filter operations in the new conversion domain, the signal expansion over the basis functions $\Phi_n(t)$ are used to represent the segmented received signal $r_m(t) = r(t - mT_s)$, $0 \leq t \leq T_c$ and the segmented receive filter $g_m(t) = g(t - mT_s)$, $0 \leq t \leq T_c$, leading to

$$r_m(t) = \sum_{n=0}^{N-1} \tilde{R}_{m,n} \Phi_n(t) \quad (19)$$

$$g_m(t) = \sum_{n=0}^{N-1} \tilde{G}_{m,n} \Phi_n(t). \quad (20)$$

Here, the new vectors $\tilde{\mathbf{r}} = [\tilde{r}_0 \dots \tilde{r}_{L-1}]^T$, $\tilde{r}_l = \tilde{R}_{m,n}$ with $l = mN + n$, and $\tilde{\mathbf{g}}_m = [\tilde{g}_0 \dots \tilde{g}_{L-1}]$ with $l = mN + n$, come from the following transformations

$$\mathbf{r} = \Psi \tilde{\mathbf{r}} \quad (21)$$

$$\mathbf{g}_m = \Psi \tilde{\mathbf{g}}_m, \quad (22)$$

where the components of the $N \times N$ transformation matrix Ψ are given by $\psi_{n,l} = \langle \Phi_n(t), \Phi_l(t) \rangle_{T_c}$ for $n, l = 1, \dots, N$. The matched filter receiver operation to estimate the j th coded bit can now be expressed as

$$\begin{aligned} \hat{a}_j &= \sum_{m=0}^{M-1} \int_{-\infty}^{\infty} r_m(\tau) g_m^*(\tau) d\tau \\ &= \sum_{m=0}^{M-1} \int_{-\infty}^{\infty} \sum_{n=0}^{\infty} \tilde{R}_{m,n} \Phi_n(\tau) \sum_{l=0}^{\infty} \tilde{G}_{m,l}^* \Phi_l^*(\tau) d\tau \\ &= \sum_{m=0}^{M-1} \sum_{n=0}^{\infty} \sum_{l=0}^{\infty} \tilde{R}_{m,n} \tilde{G}_{m,l}^* \int_{-\infty}^{\infty} \Phi_n(\tau) \Phi_l^*(\tau) d\tau \\ &= \sum_{m=0}^{M-1} \sum_{n=0}^{\infty} \sum_{l=0}^{\infty} \tilde{R}_{m,n} \tilde{G}_{m,l}^* \psi_{n,l} \\ &= \sum_{m=0}^{M-1} \sum_{n=0}^{N-1} \sum_{l=0}^{N-1} \tilde{R}_{m,n} \tilde{G}_{m,l}^* \psi_{n,l} \\ &+ \sum_{m=0}^{M-1} \sum_{n=N}^{\infty} \sum_{l=N}^{\infty} \tilde{R}_{m,n} \tilde{G}_{m,l}^* \psi_{n,l} \\ &= \sum_{m=0}^{M-1} \sum_{n=0}^{N-1} \sum_{l=0}^{N-1} \tilde{R}_{m,n} \tilde{G}_{m,l}^* \psi_{n,l} + \Gamma_j, \end{aligned} \quad (23)$$

where Γ is the truncation error. Note that the series expansion in Eqn. (23) will have to be truncated, leading to some degree of error. Although this truncation error can in principle degrade the receiver performance, we will show in the examples that any desired performance can be achieved if the trade-off between complexity, in terms of number of coefficients N , and sampling speed $\Delta F_c = 1/T_c = M/T$, is adequately set up. Note that if the basis functions are orthonormal to each other, (23) reduces to

$$\hat{a} \approx \sum_{m=0}^{M-1} \sum_{n=0}^{N-1} \tilde{R}_{m,n} \tilde{G}_{m,n}^*, \quad (24)$$

which reduces the complexity of detection. The trade-off between the choice of the basis functions, complexity of

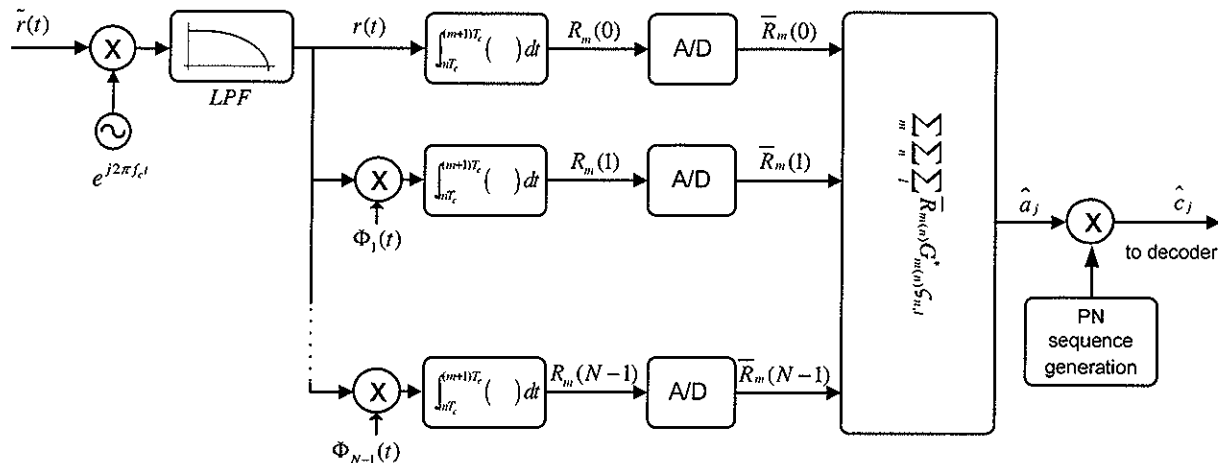


Fig. 1. Mixed-signal direct-sequence receiver block diagram.

the detection formula, and the degree of truncation error is fundamental in the receiver design.

For the all-zero code word the correlation metric (CM_1) becomes

$$\begin{aligned}
 CM_1 &= 2JE_c + \sum_{j=1}^J (2c_{1,j} - 1)(2b_j - 1)\Gamma_j \\
 &\quad + \sum_{j=1}^J (2c_{1,j} - 1)(2b_j - 1)V_j \\
 &= 2JE_c - \sum_{j=1}^J (2b_{1j} - 1)\Gamma_j - \sum_{j=1}^J (2b_{1j} - 1)V_j,
 \end{aligned} \tag{25}$$

where Γ_j , $1 \leq j \leq J$, is the truncation error due to the limited number of basis terms used in the expansion, V_j , $1 \leq j \leq J$, is the additive noise, and E_c is the chip energy. The truncation error is given by

$$\Gamma_j = \sum_{m=0}^{M-1} \sum_{n=N}^{\infty} \sum_{l=N}^{\infty} R_{m,n,j} G_{m,l,j}^* \psi_{n,l}, \tag{26}$$

The noise term is given by

$$V_j = \sum_{m=0}^{M-1} \sum_{n=0}^{N-1} \sum_{l=0}^{N-1} Z_{m,n,j} G_{m,j}^*(l) \psi_{n,l}, \tag{27}$$

where $Z_{m,n,j}$ is given by

$$Z_{m,n,j} = \int_0^{T_c} z_j(t + mT_s) \Phi_n^*(t) dt, \tag{28}$$

and $z_j(t)$ is the noise realization associated with the j th code of the received signal.

Similarly, the correlation metric for the code word C_m having weight W_m is

$$\begin{aligned}
 CM_m &= 2JE_c \left(1 - \frac{2W_m}{J} \right) \\
 &\quad + \sum_{j=1}^J (2c_{1j} - 1)(2b_{1j} - 1)(\Gamma_j + V_j).
 \end{aligned} \tag{29}$$

The probability of error is the probability that $CM_m > CM_1$ or equivalently, the probability that $D = CM_1 - CM_m \leq 0$. The difference D is given by

$$\begin{aligned}
 D &= CM_1 - CM_m \\
 &= 4E_c W_m - 2 \sum_{j=1}^J c_{mj} (2b_j - 1) \Gamma_j \\
 &\quad - 2 \sum_{j=1}^J c_{mj} (2b_j - 1) V_j.
 \end{aligned} \tag{30}$$

Both sums in Eqn. (30) have W_m nonzero components. The random variable D can be modelled as Gaussian by invoking the central limit theorem, which assumes that the weight W_m is large enough. This assumption is generally valid for PN sequences that have a bandwidth expansion of about 10 or more. Additionally, the mean of the second sum in (30) is zero because $E(2b_j - 1) = 0$, and $E(V_j) = 0$. The variance of D is given by

$$\sigma_m^2 = 4 \sum_{j=1}^J \sum_{i=1}^J c_{mi} c_{mj} E[(2b_j - 1)(2b_i - 1)] \left(\frac{E(\Gamma_i \Gamma_j)}{+E(V_i V_j)} \right), \tag{31}$$

where it has been assumed that the variables Γ_j and V_j are uncorrelated. Since the PN sequence is assumed to be uncorrelated (i.e., $E[(2b_j - 1)(2b_i - 1)] = \delta_{ij}$), (31) can be simplified as

$$\sigma_m^2 = 4W_m (E(\Gamma^2) + E(V^2)). \tag{32}$$

Let us assume that the channel remains static during the codeword. Then, the matched filter coefficients $G_{m,j}(n)$ do not depend on the code index j (i.e., $G_{m,j}(n) = G_m(n)$). The term $E(V^2)$ can be evaluated as (33) (see top of next page), where we have used $E[Z_{m_1, n_1} Z_{m_2, n_2}^*] = 0 \forall m_1 \neq m_2$. Also, $\sigma_Z^2(n_1, n_2)$ is given by

$$\begin{aligned}
 \sigma_Z^2(n_1, n_2) &= \int_0^{T_c} \int_0^{T_c} E[z(t)z^*(\tau)] \Phi_{n_1}^*(t) \Phi_{n_2}(\tau) dt d\tau \\
 &= \int_0^{T_c} \frac{N_o}{2} \Phi(t)_{n_1}^* \Phi(t)_{n_2} dt \\
 &= \frac{N_o}{2} \delta_{n_1, n_2}
 \end{aligned} \tag{34}$$

$$E(V^2) = \sum_{m_1=0}^{M-1} \sum_{m_2=0}^{M-1} \sum_{n_1=0}^{N-1} \sum_{n_2=0}^{N-1} \sum_{l_1=0}^{N-1} \sum_{l_2=0}^{N-1} E[Z_{m_1, n_1} Z_{m_2, n_2}^*] G_{m_1, l_1}^* G_{m_2, l_2} = \sum_{m=0}^{M-1} \sum_{n_1=0}^{N-1} \sum_{n_2=0}^{N-1} \sum_{l_1=0}^{N-1} \sum_{l_2=0}^{N-1} \sigma_z^2(n_1, n_2) G_{m, l_1} G_{m, l_2}^*, \quad (33)$$

where $\frac{N_o}{2}$ is the two-sided noise spectral density. Combining (33) and (34) we have

$$E(V^2) = \sum_{m=0}^{M-1} \sum_{n_1=0}^{N-1} \sum_{n_2=0}^{N-1} \sum_{l_1=0}^{N-1} \sum_{l_2=0}^{N-1} \frac{N_o}{2} \gamma_{n_1, n_2} G_{m, l_1} G_{m, l_2}^*, \quad (35)$$

The statistical characterization of Γ_j and the further simplification of (35) requires knowledge of the statistics of the received signal $r(t)$ which in turn implies knowledge of the statistics of the channel $h(t)$. We use numerical evaluation to obtain the final values of $E(V^2)$ and $E(\Gamma^2)$, and we assume that the mean of Γ is zero. Now, assuming a sufficiently long code to invoke the CLT in the detection statistic, the probability that $D < 0$ is given by

$$P(D < 0) = Q\left(\sqrt{\frac{16E_c^2 W_m^2}{E(V^2) + E(\Gamma^2)}}\right), \quad (36)$$

where $Q(\cdot)$ is the complementary error function. The energy per information bit E_b is related to the chip energy by $E_c = \frac{1}{J} E_b = R_c E_b$, where R_c is the code rate. Thus, (36) can be expressed as

$$P(D < 0) = Q\left(\sqrt{\frac{16E_b^2 R_c^2 W_m^2}{E(V^2) + E(\Gamma^2)}}\right). \quad (37)$$

Finally, the code word error probability may be upper bounded employing the union bound, yielding

$$P_e \leq \sum_{m=2}^M Q\left(\sqrt{\frac{16E_b^2 R_c^2 W_m^2}{E(V^2) + E(\Gamma^2)}}\right), \quad (38)$$

where $M = 2^J$. Note that this expression is almost identical to the probability of a code word error for soft-decision decoding of a linear binary block code in an AWGN channel, with the addition of the truncation error introduced by the limited number of basis functions in the signal expansion.

We define a receiver figure of merit, the signal to noise and truncation ratio SNTR = $\frac{16E_b^2 R_c^2 W_m^2}{E(V^2) + E(\Gamma^2)}$. The SNTR will be compared with the SNR = E_b/N_o that traditionally dominates the BER of conventional receivers. The impact of the truncation error is quantified in Section VII through simulations and it is shown that optimal performance can be obtained by adequately setting up the number of coefficients N and the segmentation factor M . We will show that the receiver degrades gracefully as the number of coefficients N is reduced, and no performance loss occurs when the truncation error becomes negligible when compared with the additive noise. This leads to a practical implementation with low complexity.

The result in (38) can be also extended to an (n, k) convolutional code, leading to

$$P_e \leq \frac{1}{k} \sum_{d=d_{free}}^{\infty} \beta_d Q\left(\sqrt{\frac{16E_b^2 R_c^2 d^2}{E(V^2) + E(\Gamma^2)}}\right), \quad (39)$$

where d_{free} is the free distance of the convolutional code and the coefficients β_d are obtained from an expansion of the derivative of the transfer function $T(D, N)$.

VII. SIMULATIONS

In this section we provide simulation results to study the impact of the interference mitigation scheme, basis truncation, mono-bit quantization, the UWB channel, and the addition of coding.

First, consider uncoded transmission in an AWGN channel. We use the second derivative of Gaussian pulse $w_{tx}(t) = \left[1 - 4\pi \left[\frac{t-T_p/2}{T_p/2}\right]^2\right] \exp\left(-2\pi \left[\frac{t-T_p/2}{T_p/2}\right]^2\right)$ as the waveform for the transmitted chip signal. The chip signal has duration T_p and carries one information bit per transmitted pulse for the uncoded simulation example. Since the 3 dB high-frequency cutoff of the transmitted pulse is roughly $3.3/T_p$, the sampling rate of a conventional all-digital time-domain implementation should be at least $F_s = 6.6/T_p$, leading to a number of samples per pulse duration equal to at least $T_p F_s = 6.6$ (or 7 samples per pulse). Taking 8 samples every T_p leads to a more conservative sampling rate. In the first set of simulations, we set $T_c = T_p$, i.e., the ADC conversion time is equal to the chip duration, so the proposed receiver samples every T_p seconds which achieves a parallel sampling rate that is 8 times slower than the Nyquist rate of the conventional time domain approach. In order to study the impact of the number of basis coefficients N , the other fundamental parameter that determines the degree of truncation error and the complexity of the system, we provide SNTR and BER simulation results.

For the first set of simulations, we use BPSK modulation and the symbols are estimated via the detection formula of Eqn. (13) without the presence of interference, where the matched filter coefficients are expansions of the transmitted pulse over the complex exponentials. We first plot in Fig. 2 the SNTR at the output of the receiver, versus the number of basis coefficients N . The plot is parameterized by the received signal SNR ($\text{SNR} = 10 \log_{10}(E_b/N_o)$) where E_b is the information bit energy which is equal to the chip energy (uncoded system), and $N_o/2$ is the two-sided noise power spectral density. The plot shows that for this case, five coefficients are sufficient to make the truncation error negligible compared with the additive noise. The same results are shown in Fig. 3 in the form of bit error rate (BER) vs. SNR parameterized by the number of expansion coefficients N . These results show that the receiver performs well even for a sub-Nyquist sampling rate ($N < 8$). For instance, at half the Nyquist rate, the receiver is only 1 dB off the optimal performance. Note that although the N coefficients are complex-valued which is equivalent to $2N$ real-valued samples, only half of these samples need to be taken from the signal expansions since the other half are complex conjugates due to the spectrum symmetry. The plot shows that the truncation error introduced

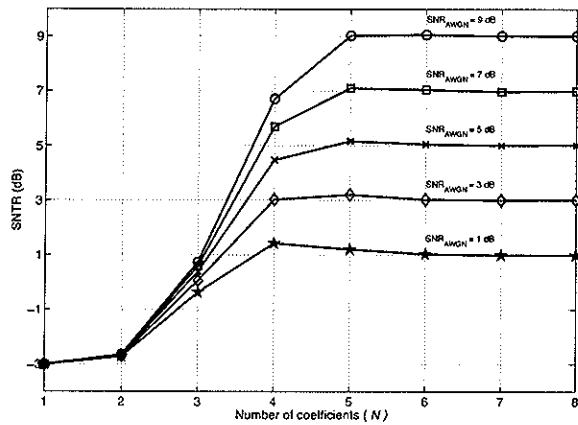


Fig. 2. Receiver output $SNTR = \frac{16E_b^2 R_c^2 W_m^2}{E(V^2) + E(I^2)}$ versus the number of basis coefficients N . $N = 5$ coefficients are sufficient for the values of $SNRAWGN = 10 \log_{10}(E_b/N_o)$ shown in the figure.

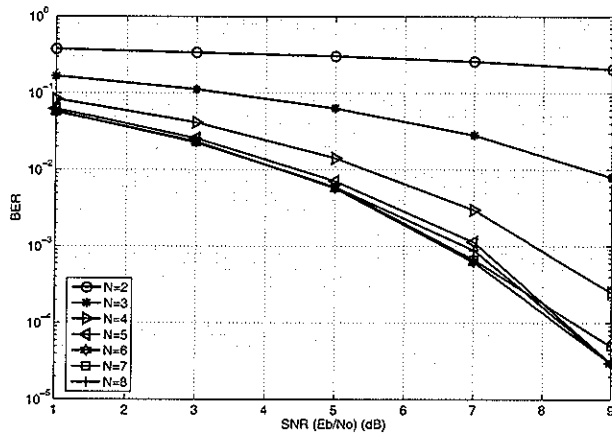


Fig. 3. Bit error rate of basic signal expansion receiver vs. SNR parameterized by the number of the frequency domain expansion coefficients N .

in the cases $5 \leq N \leq 7$ is very small compared with the additive noise for the practical range of SNR values shown in the figure. This sub-Nyquist performance shows how this sampling scheme can perform compression of the received signal at the sampling stage, and can lead to designs with reduced power and complexity.

We present next a simulation of the interference mitigation scheme introduced in Section V. The adjacent channel interference signal is a multicarrier signal with $K^{(L)} = K^{(R)}$ carriers with fixed intercarrier separation $\Delta F_c = 4.125 MHz$ and with frequency separation from baseband ΔF . We assume that these parameters are known or have been estimated. The receiver uses complex exponentials, providing frequency domain samples. The received signal is windowed with overlapping percentage $OVR=0.1$. The symbols of both the DS sequence and the multicarrier signal are estimated via the detection formula of Eqn. (12) where the matched filter coefficients are expansions of the transmitted pulse over the complex exponentials. In the simulations presented here, the frequencies of the complex exponential basis match the frequencies of the Fourier series expansion coefficients of the

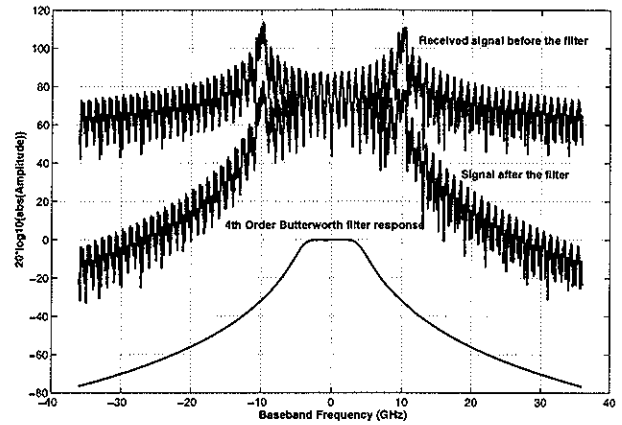


Fig. 4. Multicarrier interference before and after 4th order antialiasing filter.

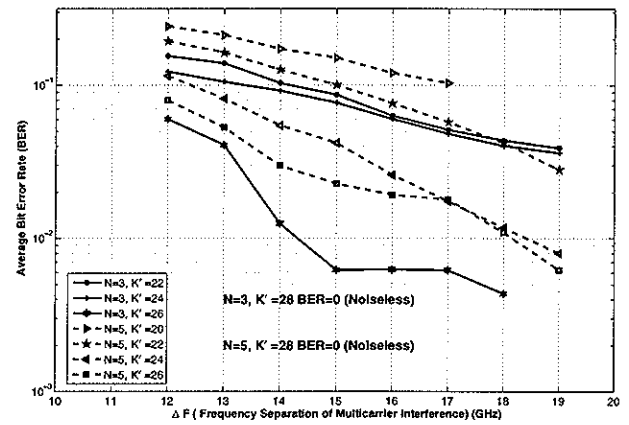


Fig. 5. BER performance vs. the frequency separation of the multicarrier interference for number of frequency samples $N = 3$ and $N = 5$ parameterized by the total estimated number of symbols $K' \leq K + 2C(K^{(L)} + K^{(R)}) = 30$, where $C = 1$ and $K = K^{(L)} = K^{(R)} = 10$. When no AWGN is added, the simulation achieves perfect symbol recovery for the cases $N = 3, K' = 28$ and $N = 5, K' = 28$ and above.

received signal. We assume that the multicarrier block has $K^{(L)} = K^{(R)} = 10$ subcarriers with QPSK modulation. These carriers are 40 dB stronger than the DS sequence. The receiver uses a 4th order Butterworth antialiasing filter. If the output of this filter is sampled at Nyquist rate by a conventional time-domain ADC, the discrete-time signal would be completely destroyed by aliasing unless the antialiasing filter can provide enough attenuation. Fig. 4 shows the frequency response of a realization of the received signal, the antialiasing filter and its filtered output signal. Fig. 5 shows the BER versus the frequency separation of the multicarrier interference channel ΔF with the number of expansion coefficients $N = 3$, and $N = 5$. The plot shows the performance penalty of the receiver as the interferer channel center frequency moves into the DS signal band. The total estimated number of symbols is $K' \leq K + 2C(K^{(L)} + K^{(R)}) = 30$, where $C = 1$ and $K = K^{(L)} = K^{(R)} = 10$. When no AWGN is added, the simulation achieves perfect symbol recovery for the cases $N = 3, K' = 28$ and $N = 5, K' = 28$ and above.

In our next simulation, we use the setup of Fig. 3, and carry

TABLE I
UWB CHANNEL MODEL 1 PARAMETERS

| | |
|---|----------------|
| Cluster arrival rate (clusters per ns) | .0233 |
| Ray arrival rate (rays per ns) | 2.5 |
| Cluster decay factor (ns) | 7.1 |
| Ray decay factor (ns) | 4.3 |
| Standard deviation of log-normal variable for cluster fading | $4.8/\sqrt{2}$ |
| Standard deviation of log-normal variable for ray fading | $4.8/\sqrt{2}$ |
| Flag for non line of sight channel | 0 |
| Standard deviation of log-normal shadowing of entire impulse response | 3 |

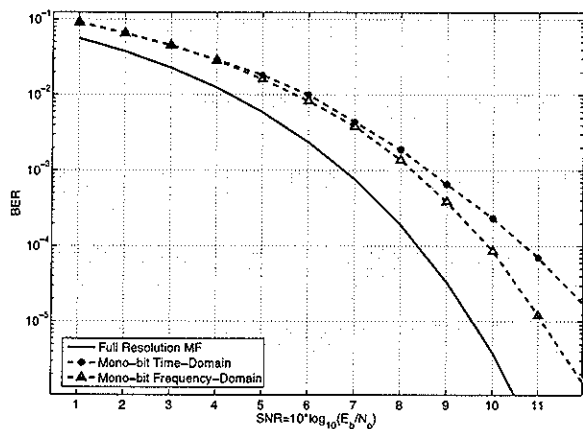


Fig. 6. Comparison between mono-bit frequency-domain, and mono-bit time-domain receiver implementations. The mono-bit frequency-domain case provides a little gain over its time-domain counterpart.

out a Monte Carlo BER estimation, shown in Fig. 6. Here, we compare with a conventional time domain implementation whose ADC is limited to one bit of resolution. The frequency domain samples are similarly quantized to a single bit, with each parallel sample taken at a rate eight times slower than the time domain sampler. We assume the receiver implements a full resolution matched filter, so only the received signal, or its basis coefficients, are quantized with a single bit. Also shown for comparison is the optimal full resolution receiver. The frequency domain approach is somewhat less sensitive to the monobit quantization, with samples provided eight times slower than the conventional receiver ADC. Note that this gain can be explained by the fact that the proposed receiver oversamples in the frequency domain by providing 5 complex-valued bits every T_p seconds (10 bits every T_p seconds) whereas the time-domain ADC would provide 8 real-valued bits every T_p seconds. However, since the signal is real-valued, the negative frequency coefficients are the complex conjugate of their corresponding positive frequency coefficients. This means that the frequency domain effectively provides 5 real-valued samples every T_p seconds, which is sub-Nyquist sampling with 37.5 % savings.

To study the impact of a multipath channel, our fourth simulation uses the UWB channel model 1 (CM1) developed by the IEEE P802.15 Working Group for Wireless Personal Area Networks. We use 100 CM1 channel realizations and calculate the SNTR vs. the number of segments (M), parameterized by different values of $\text{SNR}_{\text{AWGN}} = 10\log_{10}(E_b/N_o)$, as shown

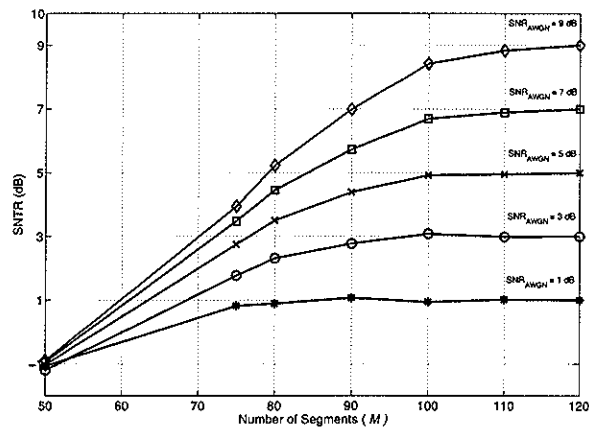


Fig. 7. Receiver output SNTR versus the number of segments M , parameterized by SNR.

in Fig. 7. The transmitted pulse is the second derivative of Gaussian, with CM1 channel parameters given in Table I. The time-domain sampling rate used in the simulations is 7 GHz, the duration of the transmitted pulse is $T_p = 1$ ns, and the received signal is processed over a time base of 100 ns. The number of expansion coefficients is $N = 7$ and the number of segments is calculated as $M = 100\text{ns}/T_c = 100\text{ns}\Delta F_c$. So, for example, if the receiver experiences an $\text{SNR}_{\text{AWGN}} = 5$ dB, a segmentation ratio of $M = 100$ (i.e., $T_c = 1$ ns) suffices to achieve Nyquist rate performance. This implies that the parallel basis coefficients are sampled at a rate of $\Delta F_c = 1$ GHz, seven times slower than a conventional time-domain implementation would utilize.

For the fifth and last simulation example, we provide the BER of the proposed receiver in combination with the $R_c = 1/2$ convolutional code $[1 \frac{1+D^2}{1+D+D^2}]$, in an AWGN channel, and using Viterbi decoding. The Viterbi algorithm is employed after despreading (see Fig. 1). Fig. 8 shows Monte Carlo BER results, with curves parameterized by number of basis coefficients N . The curves show the impact of basis truncation error on the receiver performance, and indicate that $N = 6$ is sufficient to achieve performance equivalent to a Nyquist rate conventional implementation. Note also that $N = 5$ very nearly achieves this performance, and $N = 4$ suffers only slightly more than a 1 dB loss. With $N = 6$, the basis coefficients are sampled at a rate eight times slower than the Nyquist rate for a conventional time-domain sampling approach, while requiring 6 parallel processing chains. We emphasize that for this example, when $N < 8$ the aggregate

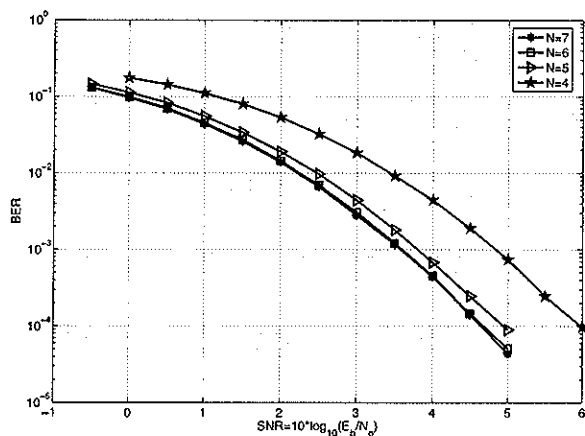


Fig. 8. BER performance employing a rate 1/2 code and the Viterbi algorithm in an AWGN channel. Curves are parameterized by the number of basis coefficients N . For $N < 8$, the aggregate sampling rate is less than the Nyquist rate.

sampling rate is sub-Nyquist. In fact, the aggregate rate can be reduced to 37.5 % that of the Nyquist rate by taking $N = 4$, at a slight loss in performance. This result is enabled by the parallel sampling and encoding.

VIII. CONCLUSIONS

We have explored a mixed-signal receiver architecture for the demodulation of UWB direct-sequence spread-spectrum signals. The receiver takes advantage of front-end mixed signal processing, using a parallel analog calculation of basis coefficients, followed by sampling and digital processing. This efficiently parallelizes the signal before sampling, and enables digital processing at a much lower rate. Time-domain signal reconstruction is not required, instead the receiver operates directly on the sampled basis coefficients. This approach helps to solve two major impediments to digital UWB receivers, namely the limited ADC sampling rate, and the need to deal effectively with large adjacent interference. In addition, distortion analysis shows that, with a coded system, the aggregate sampling rate can be considerably below the Nyquist rate of a conventional system, while maintaining BER performance.

REFERENCES

- [1] A. Papoulis, "Generalized sampling expansion," *IEEE Trans. Circuits Syst.*, vol. 24, no. 11, pp. 652–654, Nov. 1977.
- [2] S. R. Velazquez, T. Q. Nguyen, and S. R. Broadstone, "Design of hybrid filter banks for analog/digital conversion," *IEEE Trans. Signal Processing*, vol. 4, pp. 956–967, Apr. 1998.
- [3] R. M. Gray, "Oversampled sigma-delta modulation," *IEEE Trans. Commun.*, vol. 35, pp. 481–489, May 1987.
- [4] P. Aziz, H. Sorensen, and J. V. der Spiegel, "Multiband sigma-delta modulation," *Electron. Lett.*, vol. 29, no. 9, pp. 760–762, Apr. 1993.
- [5] I. Galton and H. T. Jensen, "Delta-sigma modulator based A/D conversion without oversampling," *IEEE Trans. Circuits Syst. II*, vol. 42, no. 12, pp. 773–784, Dec. 1995.
- [6] I. D. O'Donnell, M. S. W. Chen, S. B. T. Wang, and R. W. Brodersen, "An integrated, low power, ultra-wideband transceiver architecture for low-rate, indoor wireless systems," in *Proc. IEEE CAS Workshop Wireless Commun. Networking*, Sep. 2002.
- [7] S. Hoyos, B. M. Sadler, and G. R. Arce, "Mono-bit digital receivers for ultra-wideband communications," *IEEE Trans. Wireless Commun.*, vol. 4, pp. 1337–1344, July 2005.
- [8] S. Hoyos and B. M. Sadler, "Ultra-wideband analog to digital conversion via signal expansion," *IEEE Trans. Veh. Technol.*, invited, vol. 54, pp. 1609–1622, Sep. 2005.
- [9] J. G. Proakis, *Digital Communications*, 4th ed. New York: McGraw Hill, 2001.
- [10] B. M. Sadler and A. Swami, "On the performance of episodic UWB and direct-sequence communication systems," *IEEE Trans. Wireless Commun.*, vol. 3, pp. 2246–2255, Nov. 2004.
- [11] R. C. Qiu, "A study of the ultra-wideband wireless propagation channel and optimum UWB receiver design," *IEEE J. Select. Areas Commun.*, vol. 20, pp. 1628–1637, Dec. 2002.
- [12] J. T. T. Z. Xu and P. Liu, "Frequency-domain estimation of multiple access ultra-wideband signals," in *Proc. IEEE Workshop Statistical Signal Processing*, Oct. 2003, pp. 74–77.



Sebastian Hoyos was born in Cali, Colombia in 1975. He received the B.S. degree from the Pontificia Universidad Javeriana (PUJ), Bogota, Colombia in 2000, and the M.S. (2002) and Ph.D. (2004) degrees from the University of Delaware, Newark DE, all in electrical engineering. He worked for Lucent Technologies Inc. from 1999 to 2000 as Technical Manager and Sales Engineer for the Andean region in South America. Simultaneously, he was an Adjunct Professor at the PUJ University, where he lectured on microelectronics and control

theory. In the fall of 2000, he enrolled in the Department of Electrical and Computer Engineering at the University of Delaware. During his master and Ph.D. studies, he worked under PMC-Sierra Inc., the Delaware Research Partnership Program, and the Army Research Laboratory (ARL) Collaborative Technology Alliance (CTA) in Communications and Networks. In the fall of 2004, he enrolled in the Department of Electrical Engineering and Computer Sciences at the University of California, Berkeley, where he was a postdoctoral researcher at the Berkeley Wireless Research Center. He has carried out industrial consulting with Conexant Systems Inc., Red Bank, NJ. He is now an Assistant Professor at the Department of Electrical and Computer Engineering at Texas A&M University, College Station, TX. His research interests include communication systems, wireless communications, robust signal processing, and mixed-signal high-speed systems and circuit design. For a complete list of his publications and patents, please visit www.ece.tamu.edu/People/bios/hoyos.htm.



Brian M. Sadler (M'90-SM'02-F'06) received the B.S. and M.S. degrees from the University of Maryland, College Park, and the Ph.D. degree from the University of Virginia, Charlottesville, all in electrical engineering. He is a senior research scientist at the Army Research Laboratory (ARL) in Adelphi, MD. He was a lecturer at the University of Maryland, and has been lecturing at Johns Hopkins University since 1994 on statistical signal processing and communications.

He received a *Best Paper Award* (with R. Kozick) from the Signal Processing Society in 2006. He is an associate editor for the *IEEE JOURNAL ON SPECIAL TOPICS IN SIGNAL PROCESSING*, and a member of the IEEE Signal Processing Society Sensor Array and Multi-channel Technical Committee. His research interests include signal processing for mobile wireless and ultra-wideband systems, sensor signal processing and networking, and associated security issues.